

Solving mazes with single-molecule DNA navigators

Jie Chao^{1,2,8}, Jianbang Wang^{2,8}, Fei Wang^{3,4,8}, Xiangyuan Ouyang^{2,8}, Enzo Kopperger⁵, Huajie Liu^{2,6*}, Qian Li³, Jiye Shi², Lihua Wang^{2,7}, Jun Hu², Lianhui Wang¹, Wei Huang¹, Friedrich C. Simmel^{5*} and Chunhai Fan^{1,2,3*}

Molecular devices with information-processing capabilities hold great promise for developing intelligent nanorobotics. Here we demonstrate a DNA navigator system that can perform single-molecule parallel depth-first search on a ten-vertex rooted tree defined on a two-dimensional DNA origami platform. Pathfinding by the DNA navigators exploits a localized strand exchange cascade, which is initiated at a unique trigger site on the origami with subsequent automatic progression along paths defined by DNA hairpins containing a universal traversal sequence. Each single-molecule navigator autonomously explores one of the possible paths through the tree. A specific solution path connecting a given pair of start and end vertices can then be easily extracted from the set of all paths taken by the navigators collectively. The solution path laid out on origami is illustrated with single-molecule imaging. Our approach points towards the realization of molecular materials with embedded computational functions operating at the single-molecule level.

Sophisticated molecular assemblies have been previously used to create molecular machines that convert chemical, photonic or electric energy into rotary or linear movements on the nanoscale^{1–3}. In particular, DNA-based nanomachines use DNA hybridization reactions to controllably convert nanoscale Brownian motion into directed movements^{4–14}. Importantly, the base-pairing specificity and sequence-programmable nature of DNA confers a unique design flexibility to such devices. DNA-based machines have been shown to generate rotary or linear motion both in solution and on surfaces —capabilities that may find applications in such diverse areas as controlled drug release, switchable nanophotonics or the construction of artificial biomolecular motors^{15–17}. DNA nanomachines either operate autonomously by following an embedded ‘molecular program’, often a predesigned cascade reaction, or they are manually triggered via an external stimulus for each operation step.

Decision-making and other kinds of information processing may be implemented into DNA nanodevices by using concepts drawn from DNA computing, which exploits the intrinsic sequence-programmability of DNA-based reactions. Whereas the pioneering work of Adleman¹⁸ and others was still devoted to the solution of hard computational problems using molecular biology techniques, the focus of the field has shifted towards the realization of DNA-based logic circuits and dynamical reaction networks. For instance, aptamers and DNazymes have been exploited to design molecular logic gates^{19,20}. By integrating over 100 DNA logic gates, Stojanovic and coworkers fabricated an automaton named MAYA-II to play a game of tic-tac-toe²¹. More recently, there has been major progress

in the realization of reaction networks based on nucleic acid strand displacement reactions and hybridization catalysts, which have resulted in the construction of increasingly sophisticated biomolecular circuits for both in-vitro and even in-vivo computation^{20,22–25}.

DNA computing systems operating in solution rely on sophisticated sequence design to ensure that hybridization reactions occur in the correct order. In particular, specific sequence domains cannot be re-used in different contexts, which sets a limit on the complexity and scalability of such systems. To circumvent this restriction, several groups have recently developed surface-based DNA computing systems, in which DNA reaction networks are immobilized and spatially organized on micro- or nanoscale platforms^{26–28}.

Of particular relevance for the system described here, Wickham et al. demonstrated a DNA walker system driven by nicking enzymes⁹, which could be directed to take a specific path along a network of tracks laid down on a DNA origami platform. More recently, Chatterjee et al. developed an enzyme-free computing system based on the progression of hybridization chain reactions (HCR)²⁸ localized on DNA origami structures. Using bulk fluorescence spectroscopic methods for readout, they demonstrated the realization of logic gates and logic circuits, which on the platforms performed more robustly and much faster than previous systems operating in solution.

Here, we use the same basic HCR reaction scheme in a different computational context and develop a single-molecule ‘DNA navigator’ system that explores all possible paths through a tree graph defined on an origami. DNA origami structures are particularly

¹Key Laboratory for Organic Electronics & Information Displays (KLOEID), Institute of Advanced Materials (IAM) and School of Materials Science and Engineering, Nanjing University of Posts & Telecommunications, Nanjing, China. ²Division of Physical Biology and Bioimaging Center, Shanghai Synchrotron Radiation Facility, CAS Key Laboratory of Interfacial Physics and Technology, Shanghai Institute of Applied Physics, Chinese Academy of Sciences, Shanghai, China. ³School of Chemistry and Chemical Engineering, and Institute of Molecular Medicine, Renji Hospital, School of Medicine, Shanghai Jiao Tong University, Shanghai, China. ⁴Joint Research Center for Precision Medicine, Shanghai Jiao Tong University Affiliated Sixth People's Hospital South Campus, Shanghai Fengxian Central Hospital, Shanghai, China. ⁵Physics of Synthetic Biological Systems (E14), Physics Department, Technische Universität München, Garching, Germany. ⁶School of Chemical Science and Engineering, Tongji University, Shanghai, China. ⁷Shanghai Key Laboratory of Green Chemistry and Chemical Processes, School of Chemistry and Molecular Engineering, East China Normal University, Shanghai, China. ⁸These authors contributed equally: Jie Chao, Jianbang Wang, Fei Wang and Xiangyuan Ouyang. *e-mail: liuhuajie@tongji.edu.cn; simmel@tum.de; fchh@sinap.ac.cn; fanchunhai@sjtu.edu.cn

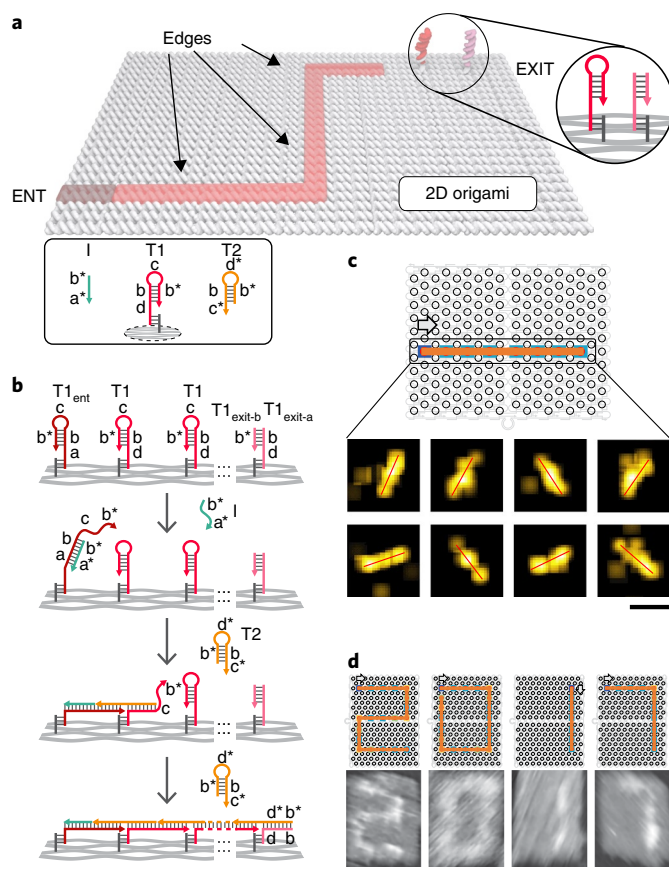


Fig. 1 | Physical implementation of the single-molecule DNA navigator.

a, Schematic illustration of the PSEC system. An acyclic connected graph (that is, a tree) is constructed on a rectangular DNA origami substrate with a size of $100 \times 70 \text{ nm}^2$. T1 and T2 are two types of fuels for driving the PSEC on the tree. Initiator I is used to trigger the initiation of the PSEC from the entrance vertex ENT. **b**, Propagation mechanism of the PSEC system. Initiator I recognizes and opens the $T1_{\text{ent}}$ hairpin at vertex ENT. The opened $T1_{\text{ent}}$ hairpin then captures and opens a T2 hairpin from the environment to start the cascade between T2 and T1. **c**, A straight line paved by PSEC and visualized with DNA-PAINT. The line has a designed length of 76 nm and is placed in the middle of a rectangular DNA origami. Alexa647-labelled anti-tags transiently bind to T2 embedded in the formed path (details are provided in Supplementary Fig. 4). **d**, Four paved digits '2', '0', '1' and '7' imaged with AFM. The T1 hairpins at the corner points have been modified to prevent unwanted spans (details are provided in Supplementary Fig. 9). The arrows indicate the propagation direction of the PSEC. Scale bars: 50 nm.

well suited for such applications, as by their very nature they are information-bearing nanostructures with well-defined geometry and nanoscale addressability^{29–38}. DNA origami has already demonstrated its great utility for the construction of molecular nanostructures resembling breadboards for prototyping of electronic circuits³⁴.

By anchoring DNA strands with carefully designed lengths and sequence domains on a two-dimensional (2D) DNA origami, we defined a simply connected maze that is equivalent to a ten-vertex rooted tree with three junctions. Exploration of the maze is provided by a proximal strand exchange cascade (PSEC) based on the HCR scheme. We demonstrate that a system composed of a large number of single-molecule DNA navigators collectively conducts a parallel depth-first search (PDFS) on the tree, and thus efficiently performs maze-solving on the 2D origami³⁹. In contrast to ref. 28, our computational approach specifically uses random search of single DNA navigators.

Working principle of the DNA navigator

Our DNA navigator is a PSEC system defined on a rectangular 2D DNA origami substrate (Fig. 1a), which consists of three components—a physical implementation of a tree graph (a representation of a ‘maze’), fuel strands and an initiator strand.

The edges of the tree were defined via anchoring sites that are constructed by site-specifically elongating a sub-set of the staple strands on the origami. Vacant areas without staple extensions correspond to ‘walls’ in the maze and block the propagation of the strand exchange cascade. One entrance and one exit are defined and denoted as vertices ENT and EXIT, respectively.

As the second component, two types of DNA hairpin are used as fuels for driving the PSEC on the tree graph. T1-type hairpins are attached along the edges and have a common sequence layout of the structure 5'-toehold-stem-loop-stem*-3' (5'-d-b-c-b*-3'); correspondingly, the T2-type hairpins, freely diffusing in solution, have a common layout of 5'-b*-d*-b-c*-3'. These two hairpins coexist metastably and fuel the PSEC process with the free energy stored in their loop regions⁴⁰. Third, an initiator strand is employed to initiate propagation of the PSEC at the entrance vertex ENT, which defines the root of the tree.

For a typical PSEC (Fig. 1b), initiator I recognizes and opens the $T1_{\text{ent}}$ hairpin at vertex ENT via base pairing between their complementary sequence domains. The opened $T1_{\text{ent}}$ hairpin then captures a T2 hairpin from solution, which subsequently unwinds the neighbouring T1 hairpin on the origami.

Similar as in Chatterjee et al.²⁸, this reaction scheme is an implementation of the HCR scheme with one of the hairpins localized to the origami platform. The following reaction cascade does not stop until all of the T1 hairpins along a path are exhausted. Of note, $T1_{\text{exit}}$ at the EXIT is designed to contain only the stem domain of the hairpin. The absence of the loop domain in $T1_{\text{exit}}$ terminates PSEC since it cannot open other T2 hairpins. According to this design, propagation of information through the network occurs only when the initiator I is present. During the propagation, the opening of a T1 hairpin by an upstream T2–T1 complex is irreversible and—upon recruitment of another T2 from solution—unidirectionally leads to the opening of the next T1 hairpin downstream. The PSEC system therefore results in a cascaded and unidirectional connection of adjacent T1 hairpins to form a long DNA path on the origami-based rooted tree with root at ENT. Only one pair of hairpin structures are needed for this system, which makes sequence design relatively straightforward.

Propagation of PSEC on origami

To test the performance of the PSEC design, we first fabricated an approximately 76-nm-long straight line on a rectangular DNA origami with a size of $100 \times 70 \text{ nm}^2$ (Supplementary Fig. 1 and see Methods). The entrance ENT was set on the left and the inter-distance between two adjacent T1 hairpins was fixed at a nominal value of approximately 10.88 nm by considering the sequence length of fuels. Purified origami sheets (5 nM) were prepared following a commonly used protocol and then mixed with a solution of T2 hairpins (500 nM). After conducting PSEC on addition of initiator I (25 nM), we observed a line on the DNA origami with a length of approximately 80 nm and a height of approximately 2 nm using atomic force microscopy (AFM) characterization (Supplementary Fig. 2). The absence of either initiator I or T2 hairpin led to no change on the origami surface (Supplementary Fig. 3). Having established the formation of a paved path from the morphological analysis by AFM, we next employed DNA-PAINT, a single-molecule super-resolution imaging technique that reveals molecular features with nanoscale resolution, to further substantiate the PSEC-based path paving. To this end, we employed a short tag sequence on T2 which allowed transient binding of Alexa647-labelled anti-tags for visualization by DNA-PAINT (Supplementary Fig. 4), which verified the formation

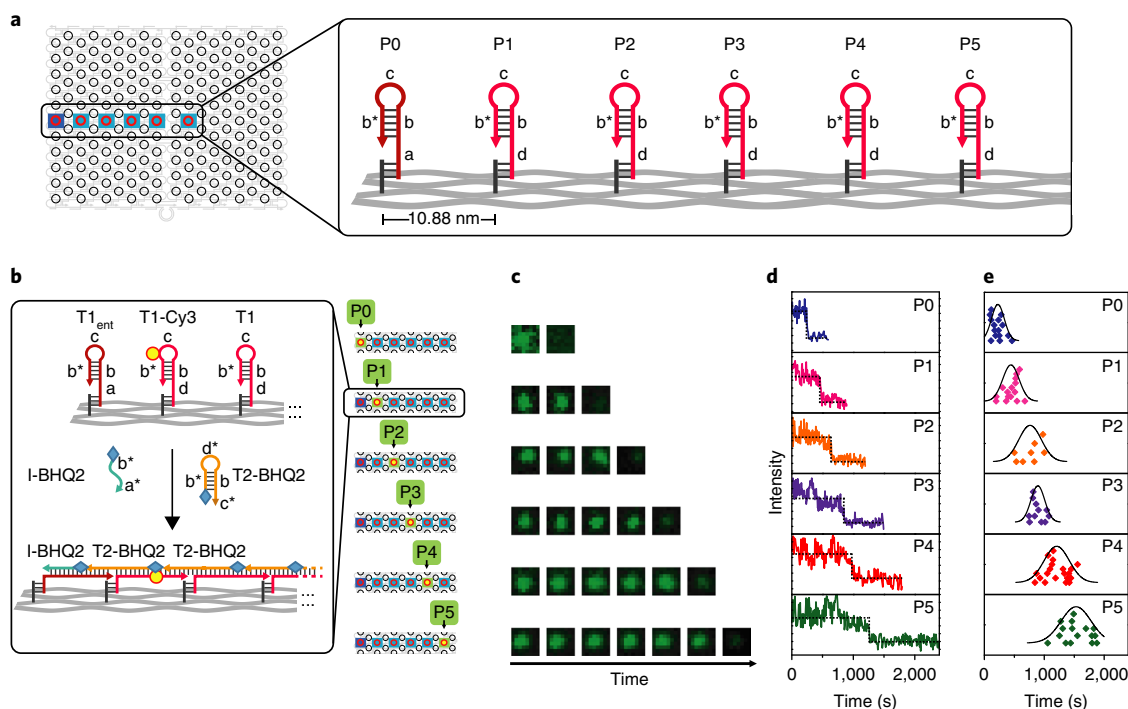


Fig. 2 | Single-molecule characterization of kinetics of PSEC. **a**, A straight line in the middle of the DNA origami was used as the testbed. Vertex P0 is the starting point and vertices P1–P5 are intermediate points. **b**, Details of the design of six parallel tests for measuring the kinetics with time-resolved TIRF. BHQ2-labelled T2 was used to quench Cy3-labelled T1 and help obtain the kinetic profile at each step. The illustrated example is used to show the mechanism of the quenching event on P1. **c**, Exemplary TIRF images showing the fluorescence changing with time of the six parallel tests. A sequence of time points of quenching from P0 to P5 could be observed. **d**, Typical single-molecule fluorescence traces for monitoring quenching events occurring at vertices from P0 to P5. **e**, Scatter plots showing statistical analysis of the length distribution for each path.

of a path with embedded T2 strands along the designed positions (Fig. 1c and Supplementary Fig. 5).

Given that the propagation of PSEC is constrained on the origami, we expected the chance of inter-origami crosstalk to be minimal. To quantify the potential occurrence of crosstalk, we deliberately mixed equal amounts of the maze origami with an interfering triangular origami structure (Supplementary Fig. 6 and see Methods). The interfering origami has a line of T1 strands but lacks the entrance vertex. Upon conducting PSEC, we found that navigation happened only on the rectangular maze origami and not on the triangular one, suggesting the high specificity of on-origami PSEC. Next, we examined also intra-origami crosstalk by customizing paths composed of multiple straight-line segments (Fig. 1d and see Methods). Due to their spatial proximity at corner points, activated T1/T2 complexes adjacent to corner hairpins may also interact with their next-nearest T1 hairpins along the path (Supplementary Fig. 7a). To avoid potentially unwanted signal propagation overriding the corner points, we optimized the strand exchange mechanism at these positions by varying the T1 and T2 sequences in their toe-hold and loop regions (Supplementary Fig. 7b). Of note, for the ‘0’ pattern, the sequence of T1_{exit} that is proximal to the starting position was optimized to ensure unidirectional clockwise propagation (Supplementary Fig. 7c). The same initiator I as before was used to trigger the PSEC, and AFM was employed for characterization. As shown in Fig. 1d, the four digits ‘2’, ‘0’, ‘1’ and ‘7’ were constructed from straight line segments, substantiating the ability of PSEC to perform a change in direction during propagation. The successful construction of complex patterns confirms the specific propagation of PSEC along prescribed paths with minimal intra-origami crosstalk. The successful navigation on the single origami with multiple crossed lines also suggests that the effect of origami bending is negligible in our setting.

The kinetics of PSEC was investigated at the single-molecule level using time-resolved total internal reflection fluorescence microscopy (TIRF). A straight-line path in the middle of the DNA origami was used as the testbed (Fig. 2a). A starting point (P0) and five intermediate steps (P1 to P5) were prescribed on the line with the same fixed spacing. We performed six parallel tests to obtain the kinetic profiles (Fig. 2b). For each test, a Cy3 dye was labelled on the loop of a T1 and a quenching group BHQ2 was labelled on the T2 or I. When a Cy3-labelled T1 hairpin was opened by a BHQ2-labelled T2 or I from solution, the fluorescence would be quenched through fluorescence resonance energy transfer (FRET). The TIRF technique enabled the examination of the cascade process in real time by continuously recording fluorescence signals (see Methods). Exemplary TIRF images shown in Fig. 2c indicate that quenching of the fluorescence occurs in the correct sequence from P0 to P5. Immediately after the addition of initiator I, the fluorescence of P0 is quenched first, reporting the start of the PSEC process. Then quenching shifts gradually from P1 to P5, consistent with the unidirectional propagation of the PSEC (Fig. 2d). Statistical analysis of each of the PSEC kinetic profiles further revealed the distribution of quenching time points at each step (Fig. 2e and Supplementary Fig. 8). Using a linear regression, we calculated the average speed of the PSEC to be 2.46 nm min^{-1} (Supplementary Fig. 9). Propagation along this straight line of 54.4 nm length thus takes approximately 22 min.

PSEC-driven graph traversal

We continued by constructing a model maze (Fig. 3a) with ten vertices (A, B, ..., J), including one entrance (vertex A), one exit (vertex J), three junctions (vertices B, D, E), one intermediate vertex (I) and four dead-ends (vertices C, F, G, H). The detailed positions of these vertices are provided in Supplementary Fig. 10a. The maze

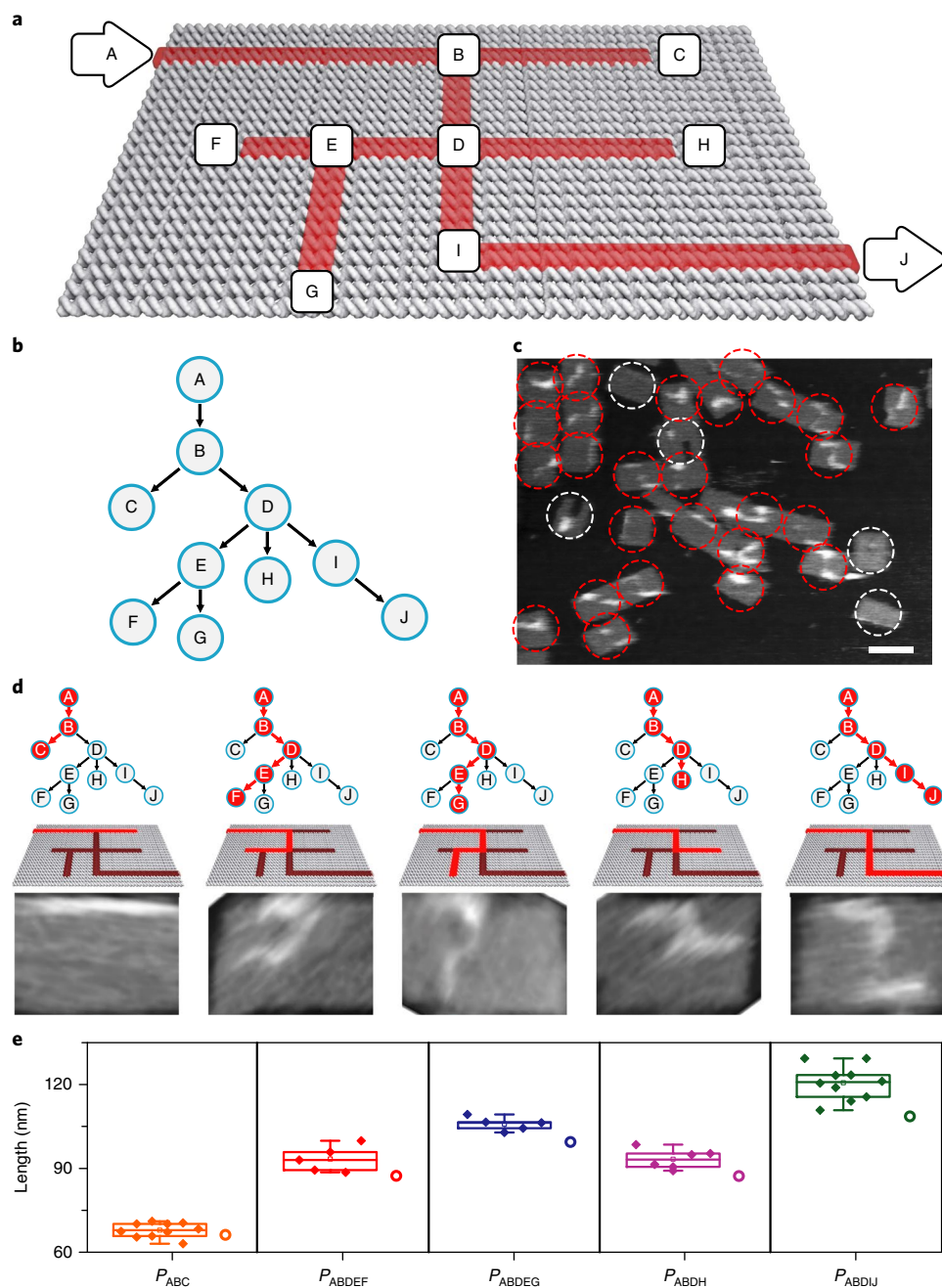


Fig. 3 | PSEC-driven graph traversal on a maze. **a**, A maze design with ten vertices. Arrows indicate the entrance vertex A and the exit vertex J, respectively. **b**, The maze is equivalent to a rooted tree with ten vertices. The entrance vertex A corresponds to the root of this tree. **c**, An AFM image showing the result of a traversal experiment that generated all possible paths. In this DNA computing implementation of a PDFS algorithm, a vast number of PSEC events occur simultaneously to realize the graph traversal on the maze. PSECs ending at the exit or at dead-ends are highlighted with red circles, invalid structures are highlighted with white circles. Scale bar: 100 nm. **d**, Typical paths found in the mixture. From left to right: paths P_{ABC} , P_{ABDEF} , P_{ABDEG} , P_{ABDH} , P_{ABDI} . Only P_{ABDI} is the correct solution to the maze. **e**, Scatter plots showing statistical analysis of the length distribution for each path. The error bars are the standard deviation for $N=10$, 5, 5, 6 and 10 samples for different paths. Circles represent theoretical lengths.

defined by this structure corresponds to a directed rooted tree with $n=10$ vertices and thus $n-1=9$ edges and root A (Fig. 3b). The tree has five leaves, of which one (J) is defined as the ‘exit’. To design the hairpin strands at the junctions in the maze, we varied the T1 and T2 sequences in their toehold and loop regions in a way similar to that in the corner design (Supplementary Fig. 10b), which prevents unwanted diagonal spans and preserves the randomness in branch selection. We examined the branch selection probability with AFM using junction patterns in this maze (see Methods). For

the ‘T’-shaped three-way junction, we found a distribution of 52.1% straight and 47.9% right-turning navigation (Supplementary Fig. 11); for the ‘X’-shaped four-way junction, the distribution is 34.5% straight, 33.1% right-turning and 32.4% left-turning navigation (Supplementary Fig. 12).

We next investigated the exploration of the vertices of the tree by the DNA navigators starting at root A. To this end, the PSEC was conducted in a solution containing 1.8×10^{10} individual mazes (corresponding to a 5 μ l volume of a 5 nM origami solution). The

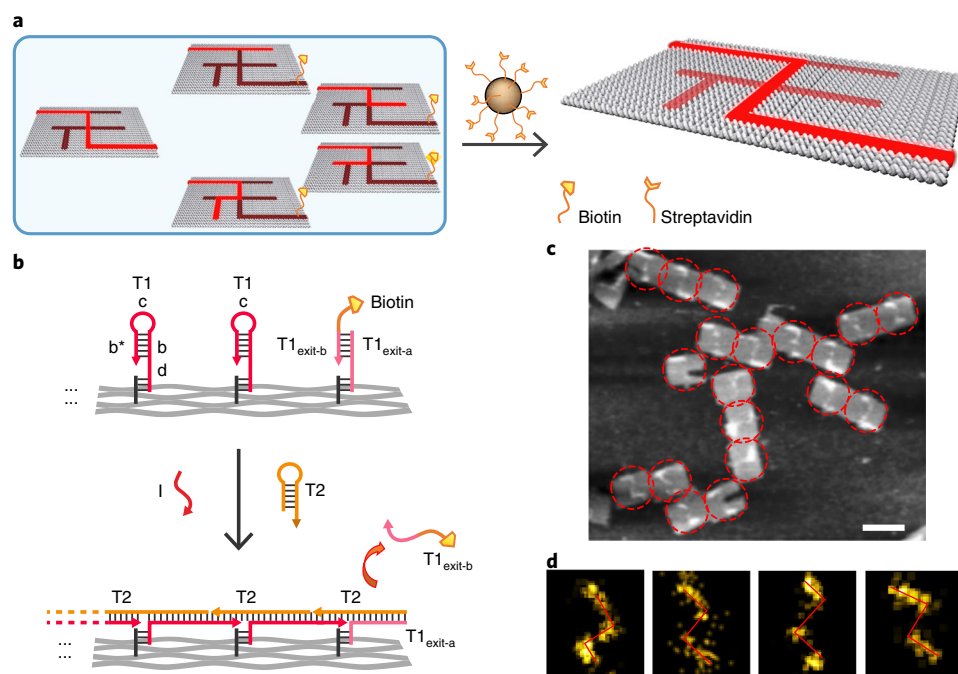


Fig. 4 | Single-molecule DNA navigators for maze-solving. **a**, Schematic illustration of magnetic bead-based selection. Exit vertex J is labelled with biotin to enable differentiation between correct and wrong paths. Only if the PSEC reaches the correct exit J, would the biotin-modified $T1_{\text{exit-b}}$ strand be released. Therefore, all wrong paths would be captured and removed by streptavidin-modified magnetic beads. **b**, Details of the release of biotin modification at the exit J by the PSEC. **c**, AFM characterization of the correct solution after selection. The remaining structures all show the correct solution path P_{ABDIJ} . **d**, Single-molecule and class-averaged DNA-PAINT characterization of the correct solution after selection. Scale bars: 100 nm in **c**; 50 nm in **d**.

$T1$ strands at junction/corner points were modified as mentioned above to prevent unwanted crosstalk and enable turning of the propagation direction in all possible directions consistent with the graph (see Methods). As confirmed by AFM imaging (Fig. 3c), the PSEC reaction produced a mixture composed of various paths formed on the mazes. Excluding those structures without any paths or with paths locked in intermediates (white circles), as expected in total five distinct paths from root A to one of the leaves were found (red circles). Four of these went to dead-ends C, F, G, H: paths P_{ABC} , P_{ABDEF} , P_{ABDEG} , P_{ABDH} ; but path P_{ABDIJ} ‘found’ the correct exit J (Fig. 3d).

In this approach, each individual PSEC progresses along one of the five possible paths. Collectively, however, all vertices of the maze are visited by the navigators. A statistical analysis of the length distribution shows that the measured path lengths coincided well with the predicted values (Fig. 3e). The probability of navigating the ‘correct’ path on the tree was examined by counting the percentage of DNA navigators successfully solving the maze (Supplementary Fig. 13). From 149 interrogated origami structures, we observed that 19 structures exhibited the correct paths, with an apparent success percentage of 12.8%. By taking account of the presence of non-completed paths caused by imperfect incorporation of staple strands²⁸, a corrected success percentage was calculated to be 14.5%, which coincides well with the theoretical prediction of 14.8% obtained with the DNA strand displacement simulator VisualDSD⁴¹ (Supplementary Fig. 14, Supplementary Note 1).

Next, we asked whether the ‘correct’ path could be selected from the mixture (Fig. 4a). To differentiate the exit vertex J from the dead-end leaves C, F, G, H, the $T1$ strand at exit J was split within the loop and a biotin modification was attached to the releasable fragment $T1_{\text{exit-b}}$ (Fig. 4b). When the PSEC reached the correct exit J, the biotin-labelled $T1_{\text{exit-b}}$ strand would be released by a $T2$ strand through a strand displacement reaction. By contrast, biotin labels would remain at J on mazes where the PSEC went to one of the dead-end

leaves. Then, streptavidin-modified magnetic beads were used to selectively remove those mazes with wrong paths. As a consequence, only mazes with the correct path (P_{ABDIJ}) would stay in solution, since they have no biotin labels at vertex J (see Methods). Characterization via AFM revealed that only the correct zigzag path was observed on all mazes after selection (Fig. 4c), demonstrating the success of this strategy. By extending the $T2$ strand with a short tag sequence for temporally docking Alexa647-labelled complementary anti-tag sequence, we could also visualize the correct path on the maze with DNA-PAINT, confirming successful solving of the maze at the single-molecule level (Fig. 4d and Supplementary Fig. 15).

Single-molecule characterization

Localizing DNA-based chemical reaction cascades onto DNA origami platforms has been previously used for the realization of autonomous DNA nanodevices and for the implementation of computational functions such as DNA-based logic circuits. With the DNA navigator system demonstrated in this work we show that proximity-based strand exchange cascades can be used in a different computational context—namely, for the exhaustive exploration of paths through tree graphs defined on the origami.

The PSEC process on the origami structures is driven by the hybridization of hairpin fuels, which are present in solution in large excess. Autonomous path exploration by the DNA navigators therefore proceeds unidirectionally, processively and essentially irreversibly. An important feature of our system is the specific design of the toehold and loop sequences of the hairpins, which enables the PSEC reaction to stochastically turn at junction and corner points of the graph defined on the origami. This enables us to implement a PDFS strategy, in which each individual DNA navigator randomly explores one of the possible paths through the given graph.

We investigated the structure and progress of individual PSEC processes using single-molecule characterization methods. Using

AFM, we were able to image paved paths on the origami structures with high spatial resolution. In addition, the super-resolution microscopy technique DNA-PAINT allowed us to characterize the trajectories taken by DNA navigators at the single-molecule level under native conditions. Since in this case imaging is based on the transient docking of dye-labelled anti-tags at the hairpin fuels embedded in the paths, DNA-PAINT also allowed verifying the path composition and further studying the propagation mechanism. Given that the strands of the PSEC can be flexibly designed, in the future the employment of multicolour DNA-PAINT could also enable the characterization of multiple orthogonal PSECs running on an individual origami structure.

From our single-molecule experiments, we were also able to determine the speed of the PSEC process. At approximately 2.5 nm min^{-1} we found the speed of PSEC comparatively rapid (Supplementary Note 2). Hence, an individual DNA navigator system can traverse a path with a length up to $1 \mu\text{m}$ —corresponding to the maximum length realizable on a standard origami rectangle—in less than 7 h. This speed is comparable to or even faster than previously achieved with nicking enzymes⁹. Of note, however, an enzyme-free approach as taken with the PSEC has less demanding buffer requirements and may therefore be applied in more diverse contexts.

Outlook

In the present work, we focused on the solution of a simply connected maze—that is, a maze without cyclic paths—as an example problem. As graph structures, such mazes are equivalent to rooted trees, where the root is the entrance to the maze, and one of the leaves is interpreted as its exit. The mazes that can be realized on a rectangular origami structure are the spanning trees of the lattice graph that is defined by the possible hairpin positions on the origami, and their subtrees. To avoid crosstalk between neighbouring paths, not all of the positions can be used, and we therefore estimate the maximum number of vertices for realistic trees to be of the order of $n \approx 8 \times 5 = 40$. The number of spanning trees of an 8×5 grid is given by 1.3×10^{15} (Supplementary Note 3). Even though this number is huge, each of these trees just has $n - 1$ edges and, by definition, at most $n - 1$ leaves and thus maximally $n - 1$ distinct paths. Thus we can expect that our DNA navigators will always explore these trees exhaustively within a few hours.

Obviously, the general requirement for graph implementation on DNA origami platforms is that they must be planar graphs. Graph exploration thus need not be restricted to acyclic graphs. However, including cycles would mean that DNA navigators can get locked up in dead ends, never reaching a given exit vertex (if there are any). In other words, performing a PSEC process on a general planar graph will always result in a self-avoiding walk on the grid. For instance, the number of only the ‘diagonal self-avoiding walks’ connecting the upper left corner of an 8×5 grid with the lower right—allowing only moves up or to the right—is $\binom{11}{4} = 330$ (Supplementary Note 3).

Rather than maze-solving, in general planar graphs we may ask for reachability of a vertex or for the shortest path between two vertices⁴². In the latter case, one could use parallel search by DNA navigators and explore the fact that the shortest paths will be traversed fastest, albeit in a stochastic manner. Here, time-dependent single-molecule characterization for tracking individual paths and statistical evaluation of solutions will be essential.

The main advantage of biomolecular computing schemes over conventional electronic computing is that they can be directly interfaced with biologically relevant processes. We therefore envisage that the translation of biomedical sensing and decision-making problems into graph representations on DNA origami platforms could be successfully applied in single-molecule diagnostics and therapeutics. For instance, tree structures can be readily used as decision trees⁴². In the context of the DNA navigator, paths through

the graphs could be selectively blocked by molecular recognition elements and thus specific output ‘leaves’ could be activated. This could be simply used as a sensor output or coupled to a molecular actuator that triggers downstream biomolecular processes.

Online content

Any methods, additional references, Nature Research reporting summaries, source data, statements of data availability and associated accession codes are available at <https://doi.org/10.1038/s41563-018-0205-3>.

Received: 8 November 2017; Accepted: 24 September 2018;

Published online: 05 November 2018

References

- Kudernac, T. et al. Electrically driven directional motion of a four-wheeled molecule on a metal surface. *Nature* **479**, 208–211 (2011).
- Hagiya, M., Konagaya, A., Kobayashi, S., Saito, H. & Murata, S. Molecular robots with sensors and intelligence. *Acc. Chem. Res.* **47**, 1681–1690 (2014).
- Kassem, S. et al. Artificial molecular motors. *Chem. Soc. Rev.* **46**, 2592–2621 (2017).
- Yin, P., Yan, H., Daniell, X. G., Turberfield, A. J. & Reif, J. H. A unidirectional DNA walker that moves autonomously along a track. *Angew. Chem. Int. Ed.* **43**, 4906–4911 (2004).
- Shin, J.-S. & Pierce, N. A. A synthetic DNA walker for molecular transport. *J. Am. Chem. Soc.* **126**, 10834–10835 (2004).
- Tian, Y., He, Y., Chen, Y., Yin, P. & Mao, C. A DNAzyme that walks processively and autonomously along a one-dimensional track. *Angew. Chem. Int. Ed.* **44**, 4355–4358 (2005).
- Gu, H., Chao, J., Xiao, S.-J. & Seeman, N. C. A proximity-based programmable DNA nanoscale assembly line. *Nature* **465**, 202–205 (2010).
- Lund, K. et al. Molecular robots guided by prescriptive landscapes. *Nature* **465**, 206–210 (2010).
- Wickham, S. F. J. et al. A DNA-based molecular motor that can navigate a network of tracks. *Nat. Nanotech.* **7**, 169–173 (2012).
- Tomov, T. E. et al. Rational design of DNA motors: Fuel optimization through single-molecule fluorescence. *J. Am. Chem. Soc.* **135**, 11935–11941 (2013).
- Cha, T.-G. et al. A synthetic DNA motor that transports nanoparticles along carbon nanotubes. *Nat. Nanotech.* **9**, 39–43 (2014).
- Kopperger, E., Pirzer, T. & Simmel, F. C. Diffusive transport of molecular cargo tethered to a DNA origami platform. *Nano. Lett.* **15**, 2693–2699 (2015).
- Yang, Y. et al. Direct visualization of walking motions of photocontrolled nanomachine on the DNA nanostructure. *Nano. Lett.* **15**, 6672–6676 (2015).
- Thubagere, A. J. et al. A cargo-sorting DNA robot. *Science* **357**, eaan6558 (2017).
- Fan, C. & Pei, H. DNA nanotechnology. *Chin. J. Chem.* **34**, 251 (2016).
- Zhou, C., Duan, X. & Liu, N. A plasmonic nanorod that walks on DNA origami. *Nat. Commun.* **6**, 8102 (2015).
- Zhu, D. et al. A surface-confined proton-driven DNA pump using a dynamic 3D DNA scaffold. *Adv. Mater.* **28**, 6860–6865 (2016).
- Adleman, L. M. Molecular computation of solutions to combinatorial problems. *Science* **266**, 1021–1024 (1994).
- Elbaz, J. et al. DNA computing circuits using libraries of DNAzyme subunits. *Nat. Nanotech.* **5**, 417–422 (2010).
- Pei, R., Matamoros, E., Liu, M., Stefanovic, D. & Stojanovic, M. N. Training a molecular automaton to play a game. *Nat. Nanotech.* **5**, 773–777 (2010).
- Macdonald, J. et al. Medium scale integration of molecular logic gates in an automaton. *Nano. Lett.* **6**, 2598–2603 (2006).
- Qian, L., Winfree, E. & Bruck, J. Neural network computation with DNA strand displacement cascades. *Nature* **475**, 368–372 (2011).
- Douglas, S. M., Bachelet, I. & Church, G. M. A logic-gated nanorobot for targeted transport of molecular payloads. *Science* **335**, 831–834 (2012).
- Han, D. et al. A cascade reaction network mimicking the basic functional steps of adaptive immune response. *Nat. Chem.* **7**, 835–841 (2015).
- Li, J., Green, A. A., Yan, H. & Fan, C. H. Engineering nucleic acid structures for programmable molecular circuitry and intracellular biocomputation. *Nat. Chem.* **9**, 1056–1067 (2017).
- Liu, H., Wang, J., Song, S., Fan, C. & Gothelf, K. V. A DNA-based system for selecting and displaying the combined result of two input variables. *Nat. Commun.* **6**, 10089 (2015).
- Boemo, M. A., Lucas, A. E., Turberfield, A. J. & Cardelli, L. The formal language and design principles of autonomous DNA walker circuits. *ACS Synth. Biol.* **5**, 878–884 (2016).
- Chatterjee, G., Dalchau, N., Muscat, R. A., Phillips, A. & Seelig, G. A spatially localized architecture for fast and modular DNA computing. *Nat. Nanotech.* **12**, 920–927 (2017).

29. Rothemund, P. W. K. Folding DNA to create nanoscale shapes and patterns. *Nature* **440**, 297–302 (2006).
30. Douglas, S. M. et al. Self-assembly of DNA into nanoscale three-dimensional shapes. *Nature* **459**, 414–418 (2009).
31. Voigt, N. V. et al. Single-molecule chemical reactions on DNA origami. *Nat. Nanotech.* **5**, 200–203 (2010).
32. Lin, C. et al. Submicrometre geometrically encoded fluorescent barcodes self-assembled from DNA. *Nat. Chem.* **4**, 832–839 (2012).
33. Kuzyk, A. et al. DNA-based self-assembly of chiral plasmonic nanostructures with tailored optical response. *Nature* **483**, 311–314 (2012).
34. Knudsen, J. B. et al. Routing of individual polymers in designed patterns. *Nat. Nanotech.* **10**, 892–898 (2015).
35. Timm, C. & Niemeyer, C. M. Assembly and purification of enzyme-functionalized DNA origami structures. *Angew. Chem. Int. Ed.* **54**, 6745–6750 (2015).
36. Edwardson, T. G. W., Lau, K. L., Bousmail, D., Serpell, C. J. & Sleiman, H. F. Transfer of molecular recognition information from DNA nanostructures to gold nanoparticles. *Nat. Chem.* **8**, 162–170 (2016).
37. Zhang, Y. et al. Transfer of two-dimensional oligonucleotide patterns onto stereocontrolled plasmonic nanostructures through DNA-origami-based nanoimprinting lithography. *Angew. Chem. Int. Ed.* **55**, 8036–8040 (2016).
38. Zhang, Z., Yang, Y., Pincet, F., C. Llaguno, M. & Lin, C. Placing and shaping liposomes with reconfigurable DNA nanocages. *Nat. Chem.* **9**, 653–659 (2017).
39. Rao, V. N. & Kumar, V. Parallel depth first search. Part I. implementation. *Int. J. Parallel Prog.* **16**, 479–499 (1987).
40. Dirks, R. M. & Pierce, N. A. Triggered amplification by hybridization chain reaction. *Proc. Natl Acad. Sci. USA* **101**, 15275–15278 (2004).
41. Lakin, M. R., Youssef, S., Polo, F., Emmott, S. & Phillips, A. Visual DSD: a design and analysis tool for DNA strand displacement systems. *Bioinformatics* **27**, 3211–3213 (2011).
42. Moore, C. & Mertens, S. *The Nature of Computation* (Oxford Univ. Press, Oxford, 2011).

Acknowledgements

We greatly appreciate financial support from the Ministry of Science and Technology of China (2016YFA0201200), National Science Foundation of China (21390414, 21473236, 21675167, 21505148, 21722310, 61771253), and the Chinese Academy of Sciences (QYZDJ-SSW-SLH031). We further acknowledge support by the Deutsche Forschungsgemeinschaft through SFB1032 Project A2 and by the Technical University Munich International Graduate School of Science and Engineering.

Author contributions

C.F. directed the research. C.F., F.C.S., H.L. and J.C. conceived the project and designed the experiments. J.C., J.W., F.W., X.O. and E.K. designed the DNA sequences, constructed the navigator system and performed the single-molecule studies. F.W., Q.L. and J.S. carried out the theoretical simulation. J.C., J.W., F.W., E.K., H.L., Lihua W., J.H., Lianhui W., W.H. and F.C.S. analysed the data. All authors discussed the results and commented on the manuscript. C.F., F.C.S. and H.L. co-wrote the paper.

Competing Interests

The authors declare no competing interests.

Additional information

Supplementary information is available for this paper at <https://doi.org/10.1038/s41563-018-0205-3>.

Reprints and permissions information is available at www.nature.com/reprints.

Correspondence and requests for materials should be addressed to H.L. or F.C.S. or C.F.

Publisher's note: Springer Nature remains neutral with regard to jurisdictional claims in published maps and institutional affiliations.

© The Author(s), under exclusive licence to Springer Nature Limited 2018

Methods

Materials. All oligonucleotides without modification were obtained from Shanghai Sangong Biotech and purified by polyacrylamide gel electrophoresis (PAGE). Fluorescently modified oligonucleotides were obtained from TaKaRa Biotechnology Co. and purified by high-performance liquid chromatography (HPLC). The DNA and primer sequences used in this work are listed in Supplementary Note 4. Single-stranded M13mp18 DNA was obtained from New England Biolabs. Streptavidin-coated magnetic microbeads were obtained from Invitrogen (product name: Dynabeads MyOne STV C1). All other chemical reagents were obtained from Sigma-Aldrich.

Preparations of DNA origami and the T1/T2-type strands. The staple strands (50 nM for each one) and M13mp18 scaffold strand (5 nM) were mixed together in $1 \times$ TAE-Mg²⁺ buffer (Tris, 40 mM; acetic acid, 20 mM; EDTA, 2 mM; and magnesium acetate, 12.5 mM; pH 8.0). The mixture was cooled from 95 °C to 20 °C at a rate of 1 °C min⁻¹ (ref. 29). After annealing, the origami solutions were purified using Amicon centrifugal filter (100 kDa molecular weight cut-off (MWCO), 3,000 g for 10 min, four times) to remove excess staple strands.

All T1/T2-type strands were annealed by holding at 95 °C for 2 min, then cooling to room temperature in 1 h (ref. 40). The T1-type strands were mixed with the purified DNA origami (10:1 in molar ratio of the T1 strands to the sites on origami) and kept at room temperature on a ThermalMixer with a mixing frequency of 300 r.p.m. overnight. Then the samples were purified using Amicon centrifugal filter (100 kDa MWCO, 3,000 g for 10 min, four times) to remove excess T1-type strands.

AFM characterizations of the samples after PSEC process. For the straight line (Supplementary Fig. 16) and the digit '1' (Supplementary Fig. 17), initiator (0.25 μM, 3 μl) and T2 strand (5 μM, 3 μl) were added into the origami solutions assembled with the T1-type strands (5 nM, 24 μl). For the digits '2' (Supplementary Fig. 18), '0' (Supplementary Fig. 19) and '7' (Supplementary Fig. 20), initiator (0.25 μM, 3 μl) and the T2-type strands (T2, 8 μM, 4 μl; T2-2, 4 μM, 2 μl) were used. The samples were kept at room temperature on a ThermalMixer with a mixing frequency of 300 r.p.m. for 2 h. Then the samples were characterized using AFM. 3 μl of the sample was dropped onto the freshly peeled mica surface and measured under tapping mode in fluid (Bruker, Multimode Nanoscope VIII) using SNL-10 probe. Two control samples of the straight line without I or without T2 strand were prepared to test the specificity of the PSEC process on the DNA origami (Supplementary Fig. 3). Another sample of straight line was prepared to measure the profile and the length of the path using DNA-PAINT. For PAINT measurements, I-P and T2-P with tags were used instead of the normal strands. Before a PAINT measurement, the sample was purified using Amicon centrifugal filter (100 kDa MWCO, 3,000 g for 10 min, four times) to remove excess I-P and T2-P strands.

For the examination of the inter-origami crosstalk, the rectangular origami mixing with an interference triangular origami (2.5 nM, 20 μl) was added with initiator (0.125 μM, 2 μl) and T2 strand (8 μM, 2 μl) (Supplementary Figs. 21, 22). For the examination of the probability of branch selection at a 'T'-shaped three-way junction and a 'X'-shaped four-way junction, initiator (0.15 μM, 2 μl) and T2 strand (12 μM, 3 μl) and T2-2 strand (3 μM, 2 μl) were added into the origami solutions assembled with the T1-type strands (3 nM, 20 μl) (Supplementary Figs. 23, 24). The samples were kept at room temperature on a ThermalMixer with a mixing frequency of 300 r.p.m. for 2 h. Then the samples were characterized using AFM.

Single-molecule characterization of the kinetics of PSEC. A straight-line path with six steps was designed to measure the kinetics of the PSEC process on the DNA origami (Supplementary Fig. 25). For that, we used TIRF to measure six different samples. For each sample, one T1-type strand labelled with CY3 was anchored at one of the six locations on the origami. The 29 mM glass bottom dishes (Cellvis, Catalog #D29-20-1-N) were pre-treated using a Harrick Plasma PDC-32G cleaner for 1 min. The diluted samples (1 nM, 10 μl) were dropped in the dish and incubated for 10 min, followed by rinsing with 100 μl $1 \times$ TAE-Mg²⁺ buffer three times. Then the initiator (0.5 μM, 5 μl) and the T2 strand labelled with BHQ2 molecule (5 μM, 5 μl) with 90 μl $1 \times$ TAE-Mg²⁺ buffer were added. The measurements were started at the same time using a laser of wavelength $\lambda = 561$ nm (150 mW, 0.3%) on a Nikon N-STORM system (exposure time, 100 ms; interval 6 s; 300 loops)⁴³. For the last two samples (the CY3-labelled T1 strand anchored on the fifth and the sixth sites, respectively), the interval was set to 8 s. Then the

videos were analysed using ImageJ and Matlab to quantify the time when the CY3 molecules were quenched by BHQ2 molecule. The velocity of the PSEC process was calculated based on the statistical data (Supplementary Figs. 8 and 9).

Maze solving. The maze was designed on the rectangular DNA origami with one entrance, one exit and four dead-ends (Supplementary Figs. 10a, 26). After the assembly of the T1-type strands on the DNA origami, the initiator (0.25 μM, 3 μl) and the T2-type strands (T2, 2 μM, 9 μl; T2-2, 2.5 μM, 3 μl) were added into the solution (8 nM, 15 μl) and kept at room temperature in a Thermomixer with a mixing frequency of 300 r.p.m. for 2 h. Then 3 μl of the sample was dropped onto the freshly peeled mica surface and measured using AFM (Bruker, Multimode Nanoscope VIII, tapping mode in fluid, SNL-10 probe).

Streptavidin-modified magnetic microbeads (MB) were used to select the correct solution for the maze²⁶. 10 μl of the MB solution was used to incubate with the DNA origami sample (4 nM, 20 μl) in $1 \times$ TAE-Mg²⁺ at room temperature for 30 min. Then the tube was set on a magnet to remove the wrong paths and the remaining sample was measured using AFM.

For the PAINT measurement of the path of the correct solution, the initiator (I-P) and the T2-type strands (T2-P, T2-2-P) with tags were used. After reaction and selecting, the sample was tested using the DNA-PAINT measurement.

PAINT measurements of the paths. For DNA-PAINT, 29 mM glass bottom dishes (Cellvis, Catalog No. D29-20-1-N) were treated with a Plasma Cleaner for 1 min in advance. The dish was incubated with 5 μl (5 nM) DNA origami and 1 μl orange Fluosphere (Life Technologies) for 8 min, rinsed with 100 μl imaging buffer gently three times, and then injected with 200 μl imager containing imaging buffer for imaging. Fluorescence spheres were used as drifted markers for the photostability. They were diluted to an appropriate concentration to ensure each imaging field has 5 to 10 of them for drift correction. 10 nt ssDNA imager labelled with Alexa647 was diluted to 10 nM in imaging buffer (5 mM Tris-HCl, 10 mM MgCl₂, 1 mM EDTA, 0.05% (v/v) Tween 20, pH 8.0).

PAINT imaging was performed on a Nikon N-STORM system. We used two excitation laser channels and one multi-bandpass filter for the detection of photons. 3% of a 647 nm laser (6 mW) was used to record the binding events of imagers and a 561 nm laser was used to monitor the drift of fluorescence spheres. The intensity of the 561 nm channel was adjusted to ensure that the fluorescence of the spheres was slightly brighter than that from bound imagers. The Andor DU-897 CCD readout bandwidth was set to 10 MHz at 14 bits and 5 \times conversion gain. EM gain was set to 100. Exposure time was chosen to be 30–100 ms so that a binding event lasted 3–5 frames on average. In total we acquired 20,000 to 50,000 frames for further analysis and super-resolution reconstruction⁴⁴.

Super-resolution rendering was performed using the ThunderSTORM plugin in ImageJ according to the user guide⁴⁵. Drift correction was performed based on the position of fluorescent spheres as drift markers. DNA-PAINT localization data were binned with a bin size of 2 nm pixel⁻¹ or 3.2 nm pixel⁻¹. Averaging was performed in Matlab by moving, rotating and overlaying reconstructed patterns within an imaging field.

Reporting Summary. Further information on research design is available in the Nature Research Reporting Summary linked to this article.

Code availability. The Visual DSD Program code used in this study is available in the Supplementary Software section of the Supplementary Information.

Data availability

All the data that support the findings of this study are available within the paper and its Supplementary Information files, and from the corresponding authors upon reasonable request.

References

- Scheible, M. B., Pardatscher, G., Kuzyk, A. & Simmel, F. C. Single molecule characterization of DNA binding and strand displacement reactions on lithographic DNA origami microarrays. *Nano. Lett.* **14**, 1627–1633 (2014).
- Jungmann, R. et al. Multiplexed 3D cellular super-resolution imaging with DNA-PAINT and Exchange-PAINT. *Nat. Methods* **11**, 313–318 (2014).
- Ovesný, M., Křížek, P., Borkovec, J., Švindrych, Z. & Hagen, G. M. ThunderSTORM: a comprehensive ImageJ plug-in for PALM and STORM data analysis and super-resolution imaging. *Bioinformatics* **30**, 2389–2390 (2014).

Reporting Summary

Nature Research wishes to improve the reproducibility of the work that we publish. This form provides structure for consistency and transparency in reporting. For further information on Nature Research policies, see [Authors & Referees](#) and the [Editorial Policy Checklist](#).

Statistical parameters

When statistical analyses are reported, confirm that the following items are present in the relevant location (e.g. figure legend, table legend, main text, or Methods section).

n/a | Confirmed

- | | | |
|-------------------------------------|-------------------------------------|---|
| <input type="checkbox"/> | <input checked="" type="checkbox"/> | The <u>exact sample size</u> (n) for each experimental group/condition, given as a discrete number and unit of measurement |
| <input type="checkbox"/> | <input checked="" type="checkbox"/> | An indication of whether measurements were taken from distinct samples or whether the same sample was measured repeatedly |
| <input checked="" type="checkbox"/> | <input type="checkbox"/> | The statistical test(s) used AND whether they are one- or two-sided
<i>Only common tests should be described solely by name; describe more complex techniques in the Methods section.</i> |
| <input checked="" type="checkbox"/> | <input type="checkbox"/> | A description of all covariates tested |
| <input checked="" type="checkbox"/> | <input type="checkbox"/> | A description of any assumptions or corrections, such as tests of normality and adjustment for multiple comparisons |
| <input checked="" type="checkbox"/> | <input type="checkbox"/> | A full description of the statistics including <u>central tendency</u> (e.g. means) or other basic estimates (e.g. regression coefficient) AND <u>variation</u> (e.g. standard deviation) or associated <u>estimates of uncertainty</u> (e.g. confidence intervals) |
| <input checked="" type="checkbox"/> | <input type="checkbox"/> | For null hypothesis testing, the test statistic (e.g. F , t , r) with confidence intervals, effect sizes, degrees of freedom and P value noted
<i>Give P values as exact values whenever suitable.</i> |
| <input checked="" type="checkbox"/> | <input type="checkbox"/> | For Bayesian analysis, information on the choice of priors and Markov chain Monte Carlo settings |
| <input checked="" type="checkbox"/> | <input type="checkbox"/> | For hierarchical and complex designs, identification of the appropriate level for tests and full reporting of outcomes |
| <input checked="" type="checkbox"/> | <input type="checkbox"/> | Estimates of effect sizes (e.g. Cohen's d , Pearson's r), indicating how they were calculated |
| <input type="checkbox"/> | <input checked="" type="checkbox"/> | Clearly defined error bars
<i>State explicitly what error bars represent (e.g. SD, SE, CI)</i> |

Our web collection on [statistics for biologists](#) may be useful.

Software and code

Policy information about [availability of computer code](#)

Data collection	Simulations were performed using VisualDSD software.
Data analysis	Data analysis and simulation was performed using VisualDSD software. The VisualDSD code used to analyse the data is provided in the Supplementary Information File, as Supplementary Software.

For manuscripts utilizing custom algorithms or software that are central to the research but not yet described in published literature, software must be made available to editors/reviewers upon request. We strongly encourage code deposition in a community repository (e.g. GitHub). See the Nature Research [guidelines for submitting code & software](#) for further information.

Data

Policy information about [availability of data](#)

All manuscripts must include a [data availability statement](#). This statement should provide the following information, where applicable:

- Accession codes, unique identifiers, or web links for publicly available datasets
- A list of figures that have associated raw data
- A description of any restrictions on data availability

All the data that support the findings of this study are available within the paper and its Supplementary Information files, and from the corresponding author upon reasonable request.

Field-specific reporting

Please select the best fit for your research. If you are not sure, read the appropriate sections before making your selection.

Life sciences Behavioural & social sciences Ecological, evolutionary & environmental sciences

For a reference copy of the document with all sections, see [nature.com/authors/policies/ReportingSummary-flat.pdf](https://www.nature.com/authors/policies/ReportingSummary-flat.pdf)

Life sciences study design

All studies must disclose on these points even when the disclosure is negative.

Sample size	Sample sizes (number of origami structures) are, in principle, very large. Experiments and data analysis were performed on subsamples large enough to gain statistically significant information.
Data exclusions	Data were only excluded for maze-solving statistics in cases where no clear path could be recognized due to origami misfolding.
Replication	All experiments were replicated at least 5 times.
Randomization	Randomization is not relevant for nanocharacterization and single molecule experiments performed with origami structures.
Blinding	Blinding is not relevant for nanocharacterization and single molecule experiments performed with origami structures.

Reporting for specific materials, systems and methods

Materials & experimental systems

n/a	Involvement in the study
<input checked="" type="checkbox"/>	<input type="checkbox"/> Unique biological materials
<input checked="" type="checkbox"/>	<input type="checkbox"/> Antibodies
<input checked="" type="checkbox"/>	<input type="checkbox"/> Eukaryotic cell lines
<input checked="" type="checkbox"/>	<input type="checkbox"/> Palaeontology
<input checked="" type="checkbox"/>	<input type="checkbox"/> Animals and other organisms
<input checked="" type="checkbox"/>	<input type="checkbox"/> Human research participants

Methods

n/a	Involvement in the study
<input checked="" type="checkbox"/>	<input type="checkbox"/> ChIP-seq
<input checked="" type="checkbox"/>	<input type="checkbox"/> Flow cytometry
<input checked="" type="checkbox"/>	<input type="checkbox"/> MRI-based neuroimaging